Proceedings of ASME Turbo Expo 2023
Turbomachinery Technical Conference and Exposition
GT2023
June 26-30, 2023, Boston, Massachusetts, USA

GT2023-102615

PERFORMANCE INVESTIGATION OF A BLADELESS AIR COMPRESSOR USING NUMERICAL SIMULATION

Ravi Nath Tiwari
TPG, University of Genoa, Italy
Email: Ravinath.tiwari@edu.unige.it

Alberto Traverso
TPG, University of Genoa, Italy

Matteo Pascenti
SIT Technologies Srl, Italy

Mario Luigi Ferrari
TPG, University of Genoa, Italy

ABSTRACT

In recent years, the demand for lightweight, compact, cost-effective, and low-noise-emission machines has increased significantly. Tesla or bladeless machines can meet the current market's demands, especially at a small scale. This article examines Tesla compressor performance numerically, which is influenced by a number of factors related to rotor and stator design. This study examines multiple aspects of Tesla's compressor in order to improve its overall performance, including the rotor, stator impact, and statorless or volute casing. An innovative bladeless rotor has been independently studied and optimized based on the Ekman number and diameter ratio. The disk gap and radius ratio are crucial to the performance of bladeless rotors. The rotor-only analysis determined an isentropic efficiency of 95%, which is in line with expectations.

An optimized rotor is initially simulated with a stator (vane diffuser) and subsequently with a volute casing. In the diffuser case, it has been numerically demonstrated that bladeless compressors can achieve an overall efficiency up to 53%. It should be noted, however, that compressor performance depends on the number of diffuser vanes and the stator-rotor interaction. With an increase in diffuser vanes, overall performance may be affected by a significant increase in frictional losses and stator-rotor interaction. In order to improve performance, the volute casing is examined, which reveals that efficiency is improved by 3%-5% as compared to the best-vaned diffuser case. Even if the final choice of the designer will depend on the performance requirements and level of complexity acceptable for the specific application, this study demonstrates that Tesla compressor with volute, i.e. statorless, overperform any vaned diffuser configuration both in terms of efficiency and pressure ratio.

Keywords: Tesla turbomachinery, Bladeless compressor, CFD.

NOMENCLATURE

C_p	Isobaric specific heat [kJ/(kg K)]
DR	Diameter ratio [-]
Diff.	Diffuser [-]
E_k	Ekman number [-]
Eff.	Efficiency [-]
h	Half disk gap [mm]
k	Specific heat ratio [-]
l	Width of disk pack [mm]
$\dot{m}$	Mass flow rate [g/s]
M	Rotor model
n	Number of disk gaps [-]
N	Rotational speed [krpm]
p	Pressure [Pa]
r	Radius [mm]
R_e	Reynolds number [-]
RT	Rotor [-]
t	Disk thickness [mm]
T	Temperature [K]
v	Velocity [m/s]
V_r	Radial velocity [m/s]
V_t	Tangential velocity [m/s]
VT	Volute Model [-]

Greek Symbol

α	Flow angle [°]
β	Pressure ratio [-]
δ	Boundary layer thickness [mm]
ε	diffuser exit/inlet ratio [-]
ρ	Fluid density [Kg/m^3]
η	Efficiency [-]
τ	Torque [Nm]
ν	Kinematic viscosity [m^2/s]
ω	Angular velocity [rad/s]

Subscripts

i	Inlet
o	Outlet
t, t-t	Total, total to total
st, t-st	Static, total to static

Acronyms

CFD	Computational Fluid Dynamics

1. INTRODUCTION

The need for compact, lightweight, efficient, low-noise and low-cost solutions proliferates worldwide in numerous industries, including the automotive sector, light aircraft, small-scale energy harvesting, and decentralized or centralized power generation [1][2][3][4][5]. A promising solution to meet such requirements at the micro-scale is represented by bladeless turbomachinery, which was introduced for the first time by Nikola Tesla (1856-1943) in 1913 [6][7]. There are many advantages of bladeless or Tesla devices, including its reversibility of operation, multiphase flow, ease of construction, low noise [8], and low cost [9][10][11][12]. Tesla-type devices consist of parallel thin flat disks that are mounted on the shaft with a specified spacer in between each disk. An illustration of the configuration of a Tesla compressor can be found in Figure 1. Through the rotation of the rotor, mechanical power is provided to the fluid, which enters axially into the hole in the rotor disk, flows through narrow radial channels traversing the disk in an outward spiral pattern due to adhesion to the surface and viscous drag between corotating disks, and exits from the disk tangentially. In response to the shear force imparted by the rotating disk, the dynamic pressure of the fluid at the disk outlet increases. In contrast to bladeless turbomachinery, conventional turbomachinery dominates the global market, but it has several disadvantages at the microscale, such as tight clearances, high frictional losses in rotors, scaling down the size efficiency drops [9][13], boundary layer loss [14], viscous effects, and high manufacturing costs associated with microblade impellers. Tesla turbomachinery may represent a viable alternative, despite being hindered by low efficiency and lack of research.

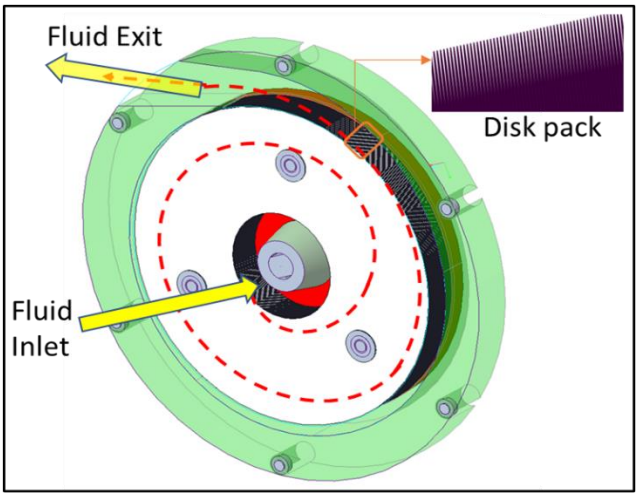

FIGURE 1: TESLA COMPRESSOR: PRINCIPLE OF OPERATION

This study aims to determine the optimal geometry of the bladeless compressor and to quantify its performance and efficiency numerically. Based on these numerical results, a Tesla compressor prototype is being developed for validation at the TPG lab, University of Genova (Italy). Tesla or bladeless expander prototypes developed at TPG lab have demonstrated the highest efficiency of 36.5% experimentally [15] with two nozzle configurations at 10000 rpm, and numerically 58% with 8 nozzle configurations at 40000 rpm [16]. Such expander prototype was also tested in reverse mode, i.e. compressor mode. A numerical study in compressor mode has achieved 43% isentropic efficiency without any modifications to the expander prototype model: such numerical results were also compared to the experimental measurements, affected by high leakage and ventilation losses [1]. As part of an effort to increase Tesla compressor performance and efficiency, rotor geometries have been independently studied based on the rotor disk gap and stator (diffuser) configurations [10].

The purpose of this paper is to investigate the performance of the innovative Tesla or bladeless compressor by numerically analyzing several aspects.

- An independent rotor analysis is carried out based on the diameter ratio as well as an optimal Ekman number and Reynolds number.
- In terms of rotor performance, the inlet and outlet flow angles of each rotor are analyzed.
- A diffuser configuration proposed by Tiwari [10] has been studied with the optimized rotor.
- A statorless (volute casing) Tesla compressor is studied with an optimized rotor, and comparisons are made with a stator-driven compressor.
- A sensitivity analysis of the number of stators (diffuser vane) is conducted to determine how overall performance is affected.

2. STATE-OF-THE-ART

There is a limited amount of literature available regarding Tesla or bladeless compressors and pumps. Among the most famous names in bladeless turbomachinery, Waren Rice was inspired by Nikola Tesla's invention. Rice [9] formulated analytical equations to describe the bladeless compressor/pumps through a first approximation technique and subsequently provided the solution through numerical computation. The efficiency of Tesla rotors was examined by varying the friction coefficient from 0.01 to 0.06 and the ratio of the outer radius to the gap. Under low mass flow rates, he obtained the highest rotor efficiency >90%. Rice designed a bladeless rotor for the Tesla compressor with 77 numbers of disks that used an outer radius of 75 mm, a thickness of 0.5 mm, and a gap of 0.5 mm. Experimental results showed that he was able to achieve a bladeless compressor efficiency of 23% at 20000 rpm and a mass flow rate of 101 g/s. Rice [13] recommended disk gaps should be twice the boundary layer thickness, still retaining laminar flow between co-rotating disks with Reynolds number in the 5 to 6 range. Crawford and Rice [17] analyzed the design of the rotor: multiple disks were the principal design problem for pumps to ensure effective diffusion of the flow as it exits the rotor. The small flow exit angle represents the main problem since it tends to hinder the following pressure recovery (low efficiency of the diffuser). In order to improve the performance of shear force pumps, Wang [18] characterized the loss of pumps with different geometry configurations at various speeds. With air as the working fluid, he predicted efficiency of 82% of the rotor, while

the maximum overall efficiency was predicted equal to 35%. Major losses occur immediately following the tip of the rotor in the cavity and the interaction between the rotor and the stator.

The Tesla turbomachinery has the advantage of being able to operate in reversible mode with minor modifications [9][16][18]. It is important to note that Tiwari [1] has numerically studied a 3 kW air Tesla prototype expander in reverse operation at different rotational speeds and he has achieved a maximum efficiency of 43% at 30000 rpm and a mass flow rate of 20 g/s (numerical). The CFD analysis revealed recirculation in the diffuser that resulted in significant pressure loss. As a matter of fact, the diffuser (compressor mode) was originally designed for the expander prototype (as a nozzle) with a divergent angle of 18.2°, which is quite aggressive for compressor mode. After comparing the numerical results with the experimental results, he found that the efficiency had been greatly reduced due to leakage. Due to the large clearance between the extreme disk and the housing, leakage was possible. However, Tiwari [1] was able to demonstrate good agreement between experimental and numerical results at very low flow regimes, with coherence in terms of maximum achievable pressures. It was noted that performance can be improved acting on several factors:

- Rotor design, disk gaps were 0.1mm, and Ekman and Reynolds's numbers were 0.8 and 2.3, respectively, which are sub-optimal values.
- Clearances between the rotor and the stator, which could be reduced.
- Clearance between the end disk and the housing, where a sealing system could be installed.
- Diffuser vanes, present high recirculation leading to losses, suggesting that an improved geometrical design would be needed.

The bladeless turbocharger patent was filed by Palumbo [19] in 2002. This patent implements a labyrinth seal to prevent air from escaping.

A study of shear force on disks pumps was conducted analytically by Hasinger [20] formulating equations (Eqs.1) governing their performance.

$$E_k = h/\delta \;=\; h\sqrt{\omega/\nu} \tag{1}$$

Hasinger's research focused on the Tesla rotor at different radius ratios (2-5), as well as the gap between disks. Interestingly, they observed a higher efficiency at a higher radius ratio at extremely low mass flow rates. A similarity parameter or Ekman number was used to evaluate the disk gap; however, the pump was designed with a radius ratio of 4 and achieved a rotor-only efficiency of 55% under experimental conditions with water as the working fluid. According to Wang [18] and Boyd and Rice [21], the flow field consists of two distinct regions, namely the entrance and the asymptotic/Ekman region. A flow velocity profile is not fully developed in the first case, while a boundary layer is fully developed in the second case.

The Reynolds number can be calculated in several ways, but the most popular method is Eqs. 2 and 3 used in Tesla turbomachinery.

$$R_e = \frac{\omega(2h)^2}{\upsilon} \tag{2}$$

$$R_{e1} = \frac{\omega r_i 2h}{\upsilon} \tag{3}$$

As a result of his numerical study of the Tesla rotor, Tiwari [10] optimized the disk gap based on Ekman number (Eq. 1) and Reynolds number (Eq. 2 and 3). The results indicated that the disk gap should be at least three times the thickness of the boundary layer, where Reynolds number based on Eq. 2 is 10 or 11 and Ekman number is 1.5-1.6. Tiwari [10] achieved the highest rotor efficiency of 82% at a low mass flow rate with an Ekman number of 1.6. In order to eliminate the diffuser recirculation issue encountered in previous studies [1], several vane geometries were investigated. A maximum total to static efficiency of 52%-53% was obtained numerically with diffuser geometrical inlet and outlet ratios of 3 in the absence of recirculation.

Wang et al. [18] conducted a numerical study involving stationary components and rotors in an effort to determine the loss mechanisms of shear stress pumps, which were primarily focused on the outlet area of the pump. At the rotor exit, highly swirled flow was observed, resulting in a high total pressure loss in the static diffuser. However, when the flow coefficient of the rotor is low and the dynamic pressure is high, the efficiency of the rotor is higher. So, a compromise between rotor efficiency and diffuser efficiency needs to be found. Wang [18] analyzed the performance drop after the outlet of the rotor numerically and experimentally. This drop was caused by strong recirculation of air in the diffuser and scroll volute, which caused reverse flow enters the rotor, causing friction loss and reducing overall performance. A Tesla compressor with a volute configuration was also investigated by Rice [9], but his studies were primarily focused on the rotor model. There was no detailed discussion of the volute configuration.

3. NUMERICAL ANALYSIS OF TESLA COMPRESSOR

This section is concerned with the numerical analysis of the bladeless compressor in 3D CFD that captures the most relevant flow phenomena occurring inside a Tesla (bladeless) compressor. The bladeless rotor is 3D numerically optimized first, then diffuser and volute with rotor configurations are 3D simulated, in order to retain sufficient accuracy with reduced computational efforts

3.1. Tesla compressor geometry and boundary conditions

In this section, Tesla compressor geometry and boundary conditions are discussed: first rotor-only configuration, second coupled rotor and stator configuration (diffuser), and third coupled rotor and volute configuration.

3.1.1 Rotor only

Since pressure is highly dependent on the radius ratio, the four rotor models in Table 1 are chosen to analyze rotor performance. Total pressure can be evaluated using Eq. (4) based on the fluid type, while maximum pressure can be calculated with Eq. (5)[22].

$$p_t = p_{max} + \frac{1}{2}\rho v^2 = \frac{\rho\omega^2(r_o - r_i)^2}{2} + \frac{1}{2}\rho(\omega r_o)^2 \quad (4)$$

$$p_{max} = \int_{r_i}^{r_o} \frac{(\rho 2\pi(2h)rdr)(\omega^2 r)}{2\pi r(2h)} \quad (5)$$

The selected designs encompass different outer diameter to inner diameter ratios (DR): the diameter ratio is 2 for M0, 2.5 for M1 and M2, and 3 for M3. Diameter ratios of 2.5 are considered twice with changes to the absolute diameter values (M1 and M2). In this analysis, the numerical study is carried out within a single disk gap while the width of the disk pack can be calculated by Eq. (6).

$$l = t(n+1) + n * 2h \quad (6)$$

For the rotor-only analysis, boundary conditions are shown in Fig. 2 (a). The full gap (2h) is chosen with a 1/8th (45°) tangential portion considered for rotor-only analysis to reduce the computational cost [1][10][16]. In order to minimize any three-dimensional effects (in the mean), a periodic boundary condition is used in the spanwise direction. For the boundary condition y = Ly/2, no-slip boundary conditions are applied.

TABLE 1: DESIGN PARAMETERS OF TESLA COMPRESSOR

Tesla Compressor				
Parameters	**Model (M0)**	**Model (M1)**	**Model (M2)**	**Model (M3)**
Disk outer diameter, mm	120	120	150	120
Disk inner diameter, mm	60	48	60	40
Diameter ratio	2	2.5	2.5	3
Disk thickness, mm	0.1			
Disks gap, mm	0.2			
Re,$(\omega(2h)^2/\nu)$	10			
E_k number, $(h\sqrt{(\omega/\nu)})$	1.6			
No of diff.1 vanes	8			
Diff.1 angle, °	3.5			
Diff.1 throat, mm	1.1			
Diff. 1 exit, (length), mm	3.3 (45)			
VTM1 duct outlet, mm	-	14.5	-	-
VTM1 diff . exit, mm	-	21.5	-	-
VTM1, outer dia., mm	-	150	-	-
Rotational speed N, krpm	40			

3.1.2 Diffuser configuration

As shown in Fig. 2 (b), a single fluid domain is considered with rotor and diffuser configuration. As a result, consider half of the disk gap *(h)* and half of the disk thickness *(t/2)* with 1/8th tangential portion (45°) in order to minimize computation costs. On one side of the fluid domain (center of gap and diffuser), the symmetry 2 boundary condition is applied, while on the other side, the symmetry 1 (diffuser) boundary condition is applied. Figure 2(b) shows a rotating wall indicated by red color. There has been a tradition of evaluating diffuser performance based on a quasi-one-dimensional theory of nozzles [23]. A performance map for a linear nozzle with a rectangular cross-section is shown in Fig. 2 (c), which is taken from Ikui (1988) and highlighted by Obayashi [23]. In the present study, however, the diffuser geometrical outlet (h_e) is 3.3 while the inlet throat (h_t) is 1.1, as shown in Table 1 which is fixed at 3.5° angle: in fact, despite nearly tangent diffusers would be theoretically desirable for Tesla compressors, manufacturing constraints require a minimum angle to be respected [13]. The diffuser is designed with a high-pressure recovery coefficient as indicated in Fig. 2 (c).

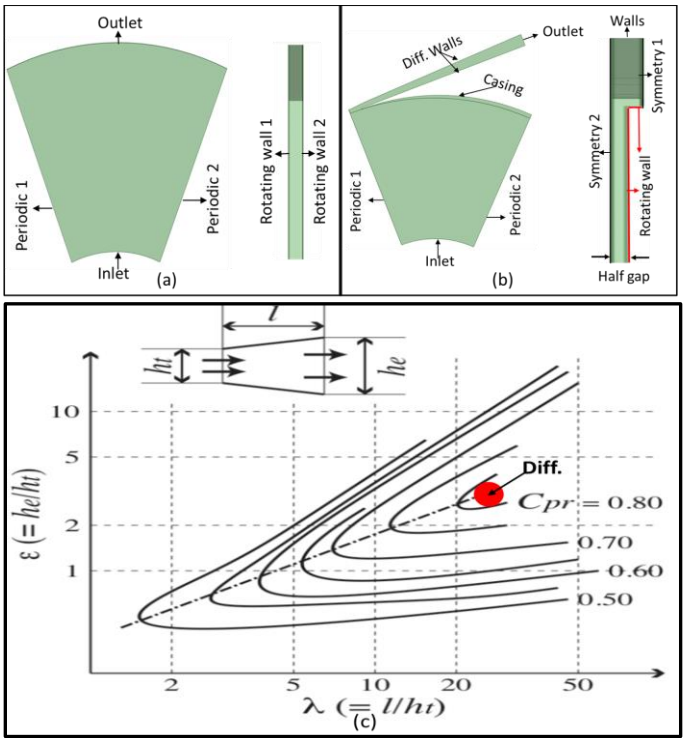

FIGURE 2: TESLA COMPRESSOR GEOMETRY AND BOUNDARY CONDITIONS FOR CFD MODELLING – (a) ROTOR ONLY (b) DIFFUSER CONFIGURATION AND (c) LINEAR NOZZLE PERFORMANCE MAP WITH A RECTANGULAR CROSS-SECTION (IKUI, 1988).

3.1.3 Statorless (Volute) configuration

Volutes perform two key functions: collection and diffusion. A compressor volute shape can have a significant impact on performance due to the non-symmetrical pressure distribution [24][25][26]. A simple calculation is done for the statorless "volute" geometry in accordance with Pan and Yu [27][28][29]. The volute geometry is analyzed with rotor model M1, where the volute outer diameter is 150 mm, and duct outlet is 14.5 mm, and the volute diffuser duct outlet is 21.5 mm. The diffusers or

volutes perform the functions of compressors by handling flow at a very small angle, making them very inefficient pumps or compressors [13]. As a consequence, the flow angle is maintained at its lowest. In this study, it has been fixed at a 3.5° angle.

For statorless analysis, both rotor and volute geometries are considered as a single fluid domain for the full circumferential domain (360°). A half-gap *(h)* and half-disk thickness *(t/2)* are taken into account when considering the volute, as shown in Fig. 3. Other boundary conditions such as symmetry, wall, and rotating wall are also considered as previous diffuser configurations in section 3.1.2.

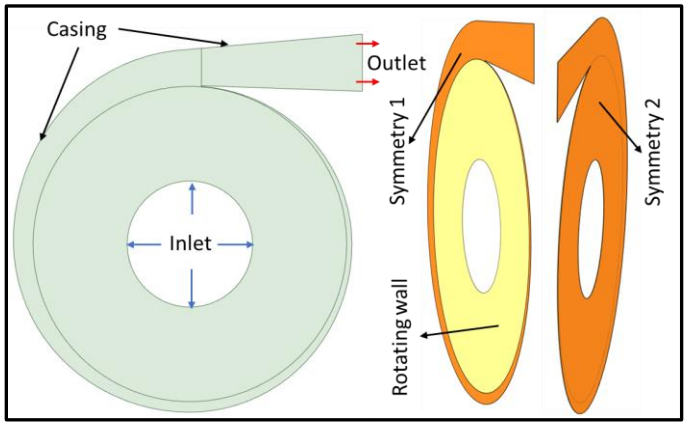

FIGURE 3: TESLA COMPRESSOR GEOMETRY AND BOUNDARY CONDITIONS FOR CFD MODELLING VOLUTE CONFIGURATION.

3.2. Numerical set-up

The numerical analysis was performed using the commercial software ANSYS FLUENT. The ANSYS program provides two types of solvers: first pressure-based and second is density-based. A density-based method was developed to solve highly compressible flows, while a pressure-based method was designed to solve flows that were incompressible or mildly compressible.[30]. However, over time it has been demonstrated that pressure-based solvers are more stable than density-based solvers when dealing with highly compressible flows [31][32] in turbomachinery applications. A density-based solver determines the density field by solving the continuity equation, while a pressure field is determined by solving the equation of state [30].

In this study, a pressure-based steady solver is selected for solving steady and compressible flows, employing ideal gas as the working fluid. The three-dimensional Reynolds Averaged Navier–Stokes (RANS) equations are discretized using the "finite volume method." The most commonly used RANS models are those defined by a pair of equations. Compared to other turbulence models, they offer an excellent trade-off between computation cost and accuracy, as demonstrated by Menter's [33] SST (shear stress transport) turbulence model in 1994. Using the SST model, it can combine the robust and accurate formulation of the k-ω model [34] in the near-wall region with the free-stream independence of the k-ω model in the far field (Menter, 1992) [33][35]. The k-ω SST viscous model is selected in this numerical study, which has become the industry standard for the analysis of turbulence. In addition, the energy equation is considered in order to take into account heat transfer in the flow field. For consideration of the temperature change caused by shear forces, the viscous heating option is selected. The compressibility effect should be enabled in pressure-based solvers when a compressible fluid is being used. The curvature option is also enabled in order to capture accurate results near the edge of the carve.

For solving the governing equations, a coupled scheme for fluid coupling of pressure and velocity is used. The coupled scheme has some advantages over non-coupled approaches. This scheme provides a robust and efficient single-phase implementation for steady-state flows, exhibiting superior performance to segregated schemes. This scheme is based on a second-order linear interpolation upwind. The flow domain between two rotating disks is considered to be stationary. When considering the entire "rotor-diffuser" and "rotor-volute" configuration, half of the thickness of the disk and half of the gap between rotating disks are considered to be a single fluid domain. The boundary conditions for temperature (300 K) and total pressure (atmospheric) have been set at the inlet, whereas the mass flow boundary condition has been set at the outlet [1][10] [36]. The rotating wall is considered a moving wall with no-slip conditions. The standard roughness model (sand-grain roughness constant-0.5) is considered on both moving and stationary walls. Inflation layers are applied on both stationary and moving walls The facet average wall function y+ values are maintained as recommended by the k-ω SST model. It is recommended to use a facet average y+ value of less than 1 for this model, but this value may be less than 5 depending on the complexity of the case [37].

3.3. Grid generation

This study examines the generation of meshes for the Tesla rotor only, diffuser "rotor-stator" and statorless configuration "rotor-volute". A hexahedral mesh is generated for the rotor, while polyhedral meshes are generated for the stator and stateless configuration as shown in Fig. 4. Mesh sensitivity analysis is performed from coarse to fine cells for accurate analysis as shown in Table 2. Hexahedral meshes are generated exclusively for the rotor as shown in Fig. 4 (a), ranging from 17005 to 202882 cells, with a final selection of 202882 cells with almost minimal error for pressure, torque, and mass flow rate. The stator and stator-less configurations generate a tetrahedral mesh that is converted into a polyhedral mesh using the ANSYS FLUENT software as shown in Fig. 4 (b and c). Polyhedral elements have become increasingly popular as alternatives to tetrahedral elements [30][38]. A polyhedral structure has the advantage of having more adjacent neighboring cells than a tetrahedral structure. Since polyhedral meshes have more nodes and faces per cell, as well as more neighbors, there is a greater number of computations per cell [38]. However, this is offset by the fact that convergence takes place within a shorter period of time. In order to determine the sensitivity of the stator configuration, 972476

cells are considered with 0.57%, 0.2%, and 0.098% change for static pressure, torque, and mass flow rate respectively. In the case of a statorless (rotor and volute) configuration, 1263827 cells are considered with a change of less than 0.5% in all static pressure, torque, and mass flow rate conditions.

TABLE 2: GRID INDEPENDENCE ANALYSIS

Mesh model #	# Nodes	# Element	Total pressure (Pa)	% Change	Torque (Nm)	% Change	Mass Flow (g/s)	% Change
Rotor only - Hexahedral mesh								
1	34560	17005	71324	-6.77%	0.000366	-1.80%	0.02481	-0.751%
2	51042	25200	71405	-6.65%	0.000366	-1.77%	0.02490	-0.390%
3	104152	51612	72550	-4.96%	0.000365	-2.00%	0.02512	0.471%
4	208146	137700	76050	-0.13%	0.000373	0.01%	0.02503	0.109%
5	306252	202882	76150		0.000373		0.02500	
Diffuser configuration (Rotor+Stator) - Polyhedral mesh								
Mesh model #	# Nodes	# Element	Static pressure (Pa)	% Change	Torque (Nm)	% Change	Mass flow (g/s)	% Change
1	397228	145660	41770	-0.93%	0.0004360	-1.577%	0.03000	-0.079%
2	736649	260331	42440	0.66%	0.0004324	-2.418%	0.03008	0.184%
3	1266714	441190	42400	0.57%	0.0004420	-0.209%	0.03000	-0.098%
4	2840156	972476	42160		0.0004429		0.03003	
Statorless configuration (Rotor + Volute) - Polyhedral mesh								
1	1690842	756386	40175	-5.85%	0.0068652	6.27%	0.449997	-0.0007%
2	1549122	328173	41100	-3.47%	0.0064050	-0.47%	0.449999	-0.0002%
3	2202884	456693	42250	-0.65%	0.0064114	-0.37%	0.449996	-0.0009%
4	3464166	711906	42300	-0.53%	0.0064167	-0.29%	0.449998	-0.0004%
5	6241187	1263827	42525		0.0064349		0.450000	

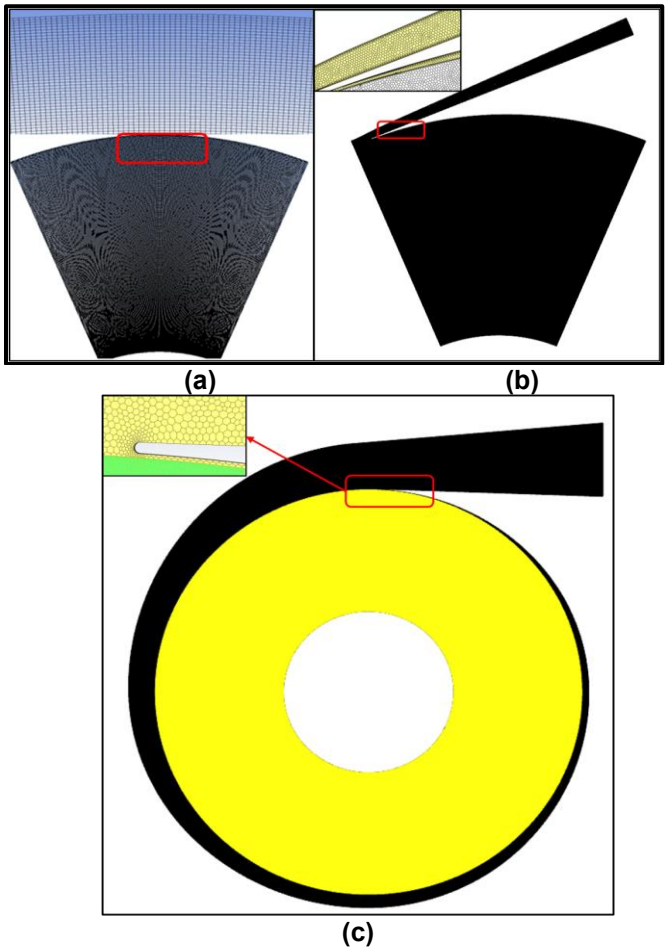

FIGURE 4: TESLA COMPRESSOR: GENERATED MESH – (a) ROTOR ONLY (b) DIFFUSER CONFIGURATION AND (c) VOLUTE CONFIGURATION

4. RESULTS AND DISCUSSION

In this section, Tesla compressor numerical results are discussed for all three configurations: rotor only, rotor-stator, and rotor with volute configurations.

4.1. Independent rotor analysis

In order to conduct independent rotor analyses with a single disk gap, four-rotor models are considered: M0, M1, M2, and M3 as shown in Table 1. As illustrated in Figure 5, the total to total pressure ratio is plotted against the mass flow rate. The total pressure is taken using the mass-weighted average method and pressure ratio is calculated by Eq.(7).

$$\beta_t = \frac{p_{t-o}}{p_{t-i}} \tag{7}$$

Based on the results, it appears that pressure ratios are highly dependent on area, as shown in Figure 5. In all four models, there is a sharp increase in pressure ratio at low mass flow rates, which was also highlighted by other authors[1][9][13][18]. Due to its 150 mm outer diameter, M2 (DR-2.5) indicates a total to total pressure ratio of 2.6, higher than the other models which have 120 mm outer diameter. The models M0, M1, and M3 have a fixed outside diameter of 120 mm with variations in their inlet sections. Nevertheless, the higher diameter ratio implies a bit higher pressure ratio than the lower diameter ratio. As the mass flow increases, model M3 (DR-3) decreases with a bit higher gradient than M1 and M0. In the case of the M3 (DR-3) and M1 (DR-2.5), the maximum total pressure ratio is 1.95 and 1.91 at 0.04 g/s mass flow rate, respectively.

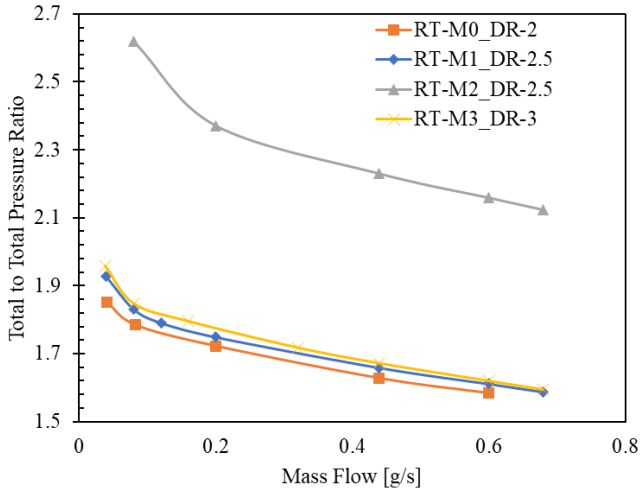

FIGURE 5: ROTOR-ONLY; TOTAL TO TOTAL PRESSURE RATIO VS MASS FLOW RATE FOR DIFFERENT DIAMETER RATIOS

Figure 6 illustrates the relationship between total to total efficiency and mass flow rate for Tesla rotor models. The total to total efficiency is calculated by using Eq.(8). C_P, the specific heat at constant pressure, and k, the heat capacity ratio, are constant with temperature. The C_P value for air is 1.005 kJ/kg K, and the

k value is 1.4. There are several averaging methods but in this study, the mass-weighted average method is considered [39].

$$\eta_{t-t} = \dot{m}\, C_P\, T_{t-i} \frac{\beta_t^{\frac{k-1}{k}} - 1}{\tau\, \omega} \tag{8}$$

Many authors[1][9][13][21] have predicted that the efficiency of rotors can reach more than 90%. In fact, thanks to the choice of the optimal Ekman number equal to 1.6 for all rotor models to use the optimal gap between disks. This CFD study predicted at low mass flow rates of 0.04 g/s, rotor efficiency reached a maximum of >95% for the diameter ratios 2.5 and 3 (M1 and M3) while M2 at 0.8 g/s. It has been studied numerically by Tiwari [10] that bladeless rotors with diameter ratios of 2 (M0) and an optimal disk gap of 0.2 mm produce a maximum efficiency of 82.5%. Models M1 and M2 have a diameter ratio of 2.5, with an outer diameter of 150 mm and 120 mm, respectively. As M2 has a wider area than M1, it indicates a higher efficiency at higher mass flow rates, but both models indicate >95% efficiency. As a result of the diameter ratio 3, the M3 predicted a bit higher efficiency at low mass flow rates, but as the mass flow rates increase, the efficiency decreases with higher gradients as compared to the diameter ratio 2.5 of the M1. Nikola Tesla [6][7] claimed a bladeless rotor efficiency of around 97% which is possible to be obtained just at a very low mass flow rate. The performance of bladed compressors is evidently affected by a decrease in rotor diameter, whereas in bladeless turbomachinery the performance and efficiency are not significantly affected by scaled-down sizes [9]. Due to this working principle, viscous loss affects the performance of bladeless compressors by increasing the mass flow rate.

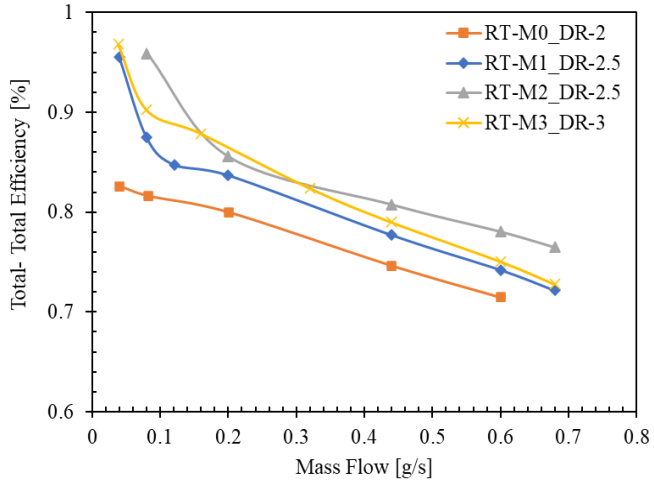

FIGURE 6: ROTOR ONLY - TOTAL TO TOTAL EFFICIENCY VS MASS FLOW RATE FOR DIFFERENT DIAMETER RATIOS

Figure 7 illustrates the relationship between the inlet and outlet flow angle and the mass flow rate: 0° corresponds to the radial direction. As the bladeless rotor spins at 40000 rpm, the tip velocity is significantly higher as the radius of the rotor increases. In this case, the pressure ratio line is asymptotic to the y-axis, whilst the bladed compressor is generally asymptotic to the x-axis. The results of this study are quite interesting at first glance, and they explain the advantages of bladeless turbomachinery. Despite varying mass flow rates, the flow can adapt to the optimal flow angle due to the absence of blades, which results in high performance every time [10]. The mass-weighted averaging method uses for the velocities and flow angle evaluated using Eq.

$$tan\,(\alpha_o) = \frac{V_{t\_o}}{V_{r\_o}} \tag{9}$$

As a result of a very low mass flow rate of 0.04 g/s (highest rotor efficiency obtained), the outlet flow angle is approximately 89.92°, i.e. almost 90°. When the mass flow rate is low, the flow angle is almost tangential, but as the mass flow rate increases, the flow angle drops, which is caused by an increase in radial velocity. Despite this, maintaining an almost tangential flow angle at higher mass flow rates is challenging for achieving higher efficiency when a diffuser will be coupled. However, the M2 model is predicted to have a higher flow angle in relation to increasing mass flow when compared to M1 and M3. Therefore, a flow angle of around 90 degrees is required for optimum efficiency of rotor-only. It is estimated that the outlet flow angle at the peak rotor efficiency point is 89.92° (almost tangential). This flow angle is quite difficult to maintain in a stator configuration. When the mass flow rate is increased, there is a 15%-18% drop in rotor efficiency with a 2° change in outlet flow angle.

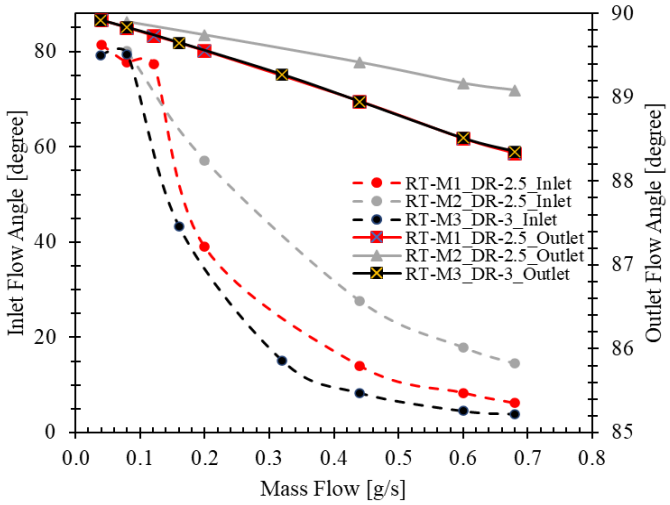

FIGURE 7: ROTOR-ONLY INLET (DASHED LINE) AND OUTLET (SOLID LINE) FLOW ANGLE VS MASS FLOW RATE FOR DIFFERENT DIAMETER RATIOS

In conventional turbomachinery generally [40][41][42][43] it should be noted that IGV (inlet guide vane) can also improve the performance of turbomachinery such as fans, compressors, and pumps. In bladeless turbomachinery, there are no flow guiders and inlet nose cones.

The flow angle at the inlet of the bladeless compressor is also studied in order to analyze its impact on its performance. The inlet flow angle is calculated using Eq.(10).

$$tan\ (\alpha_i) = \frac{V_{t\_i}}{V_{r\_i}} \tag{10}$$

A flow guide is not present in the inlet section, which means that the flow practically enters axially so that the extra-axial fluid domain is considered. The flow is entering almost axially and moves spirally between disks and exits radially. Using the inlet tangential and radial velocities, the flow angle is determined that the maximum is around 80° at a mass flow rate of 0.04 g/s. As the mass flow rate increases, the inlet flow angle drops suddenly, resulting in an increase in radial velocity and a decrease in tangential velocity, as expected. However, a low inlet flow angle may be able to have some effect on the overall performance. However, the implementation of the conical flow guider would enable the flow to enter not in a pure axial but with a mix of radial and axial flows. In addition to reducing the inner radial velocity utile the extreme disk. By increasing the flow guider length, the total to static efficiency can be improved by reducing the radial inlet velocity towards the extreme disk, which could improve the overall performance by some amount. It is expected that such studies will be analyzed in the near future in order to minimize inlet losses.

4.2. Tesla compressor analysis with stator (diffuser) and statorless (volute) configuration

In this section, numerical analysis is performed for stator (vane diffuser) and statorless configurations for M0 (DR 2), M1 (DR 2.5), and M2 (DR 2.5) geometries. The rotor model > DR-2.5 exhibits better performance at low mass flow rates and decreases in performance with a high gradient as the mass flow rate increases. Therefore, the rotor considered the rotor model M1 DR-2.5 in order to analyze the performance of the diffuser (8-numbers) and volute configuration at higher mass flow rates because it has a lower gradient as compared to rotor model M3 (DR-3). An illustration of the total to static pressure ratio and mass flow rate for the stator (vaned diffuser) and statorless (volute) configurations with rotor model M1 is shown in Fig. 8. According to the results, the ratio of total to static pressure increases as the mass flow rate decreases. The highest pressure ratio of 1.75 is shown for model M2 at 0.55 g/s, which can be compared to the M1 highest pressure ratio of 1.4 at 0.6 g/s: the different values are mainly due to the higher tip speed of M2 than M1. The Total to static pressure ratio is calculated by Eq. (11) using the mass-weighted average method.

$$\beta_{t-st} = \frac{p_{st-o}}{p_{t-i}} \tag{11}$$

With regards to volute, results are provided for the rotor model M1 (DR2.5). A volute tongue is generally the "start" of the volute, which area increases as more flow is added in the direction of rotation [30][25][43]. When approaching the tongue from the other side, the objective is to prevent the flow from being recirculated. The volutes tend to perform worse in flow rates that are greater than or less than their design point, much like impellers, which have a design point flow at which they are most efficient [43]. Comparing the diffuser case (diff1) and the volute case (VTM1), the volute model allows the maximum pressure ratio to increase from approx. 1.45 to 1.48 and the curve of the volute model (VTM1) has a low gradient as opposed to that of the diffuser model: furthermore, the volute compressor shows a characteristic curve shifted to higher mass flow values, which is beneficial in terms of system compactness by reducing the number of disks and gap. The mass flow is continuously added in the rotational direction of the volute casing, which results in a higher pressure ratio and an avoidance of recirculation. It is also possible for such a bladeless device to prevent surge events: this aspect needs further investigation. According to Rice's [9] study at different rotational speeds, they found a higher pressure ratio at very low mass flow rates, which is not common in conventional compressors, prone to surge after a minimum mass flow rate. When the mass flow rate is 1.2 g/s, the Mach number for the volute configuration is less than 0.9, so increasing the mass flow rate further the volute configuration will enter choke conditions.

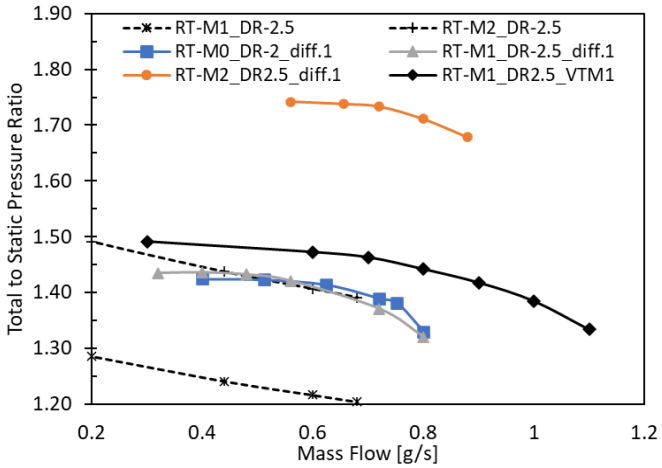

FIGURE 8: TOTAL TO STATIC PRESSURE RATIO VS MASS FLOW RATE FOR DIFFERENT ROTOR (DASHED LINE) MODELS AND ROTOR WITH DIFFUSER & VOLUTE CONFIGURATIONS (SOLID LINE)

As shown in Figure 8, the dashed line indicates the total to static pressure ratio for the rotor models M1 (DR-2.5) and M2 (DR-2.5), whereas the solid line indicates the total to static pressure ratio for the entire configuration i.e. rotor with diffuser and volute configuration. Basically, this is the analysis of the rise in static pressure between the rotor and stator, or between the rotor and volute. Static pressure increases with decreasing mass flow rate due to an increase in enthalpy for both stator and volute configurations. A higher total-static pressure ratio is observed at a low mass flow rate for rotor models M1 and M2, as indicated by the dashed line in Figure 8. Rotor and sator rise static pressure differences are 1.5 to 1.8 times the rotor static pressure, while in the volute configuration, they are 1.8 to 2.15 times. The static

pressure rise is improved in the volute case compared to the stator case. It is noted that the static pressure rise in the volute configuration is greater than two times the static pressure rise in the rotor peripheral when the mass flow rate is higher at the outlet and decreases somewhat as it approaches lower mass flow rates. It is due to the working principle of bladeless compressors that they show higher performance at lower mass flow rates, while conventional compressors are characterized by lower performance.

Figure 9 illustrates the total to static efficiency vs mass flow rate. When the diffuser configuration is used, the maximum total to static efficiency is 53.5%, whereas the volute configuration VTM1 is found to have a higher efficiency around 55.5% at a higher mass flow rate. The total to static efficiency is calculated by Eq. (12).

$$\eta_{t-st} = \dot{m}\, C_P\, T_{t1} \frac{\beta_{t-st}^{\left(\frac{k-1}{k}\right)} - 1}{\tau\, \omega} \qquad (12)$$

It is evident that the diffuser configuration differs by 1-2 % in efficiency from the rotor models M0 and M1, which indicates that the diameter ratio plays an imperative role in the bladeless compressor efficiency, rather than on pressure ratio and mass flow, whereas, indeed, plays a less significant role. A bit higher rotor efficiency is indicated by the rotor model M3 (DR 3) as compared with DR-2.5. However, the higher diameter ratio increases the efficiency but specifically in a specific very low mass flow rate and the higher diameter ratio curve decreases with a higher gradient as the mass flow rate increases. Therefore, in this study, it is estimated that diameter ratios of 2.5 and 3 are suitable for obtaining maximum efficiency. In the overall analysis of rotor and stator performance, the rotor model 1 (DR-2.5) is selected to analyze efficiency at a higher mass flow rate, since it has a lower gradient than the rotor model 3 (DR-3).

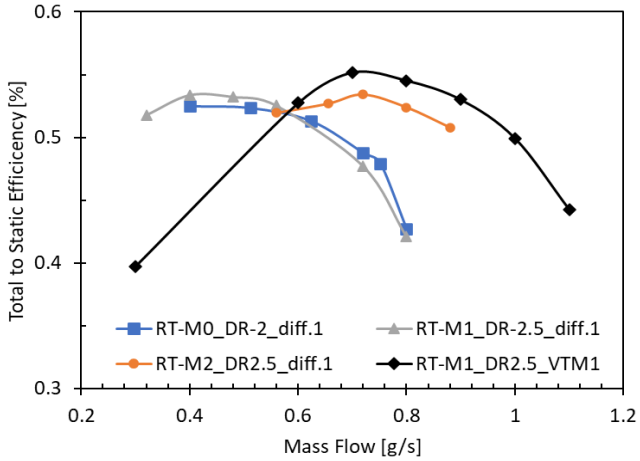

FIGURE 9: TOTAL TO STATIC EFFICIENCY VS MASS FLOW RATE FOR DIFFERENT COMPRESSOR (WITH DIFFUSER AND VOLUTE) CONFIGURATIONS

The fact that rotor efficiency is higher at low mass flow rates has been discussed in section 4.1, whereas with stator and volute configurations, efficiency is likely to be reduced by the interaction between the rotor and the stator. Many authors have observed that rotor efficiency is high but performance falls heavily just after the rotor or when the stator has interacted with the rotor [1][9][13][18]. Due to rotor and stator interaction, efficiency decreased by>15%, whereas rotor efficiency is > 78% at 0.4 g/s. As a result of the use of the volute, the rotor-to-stator interaction losses are minimized, resulting in an overall improvement in efficiency > 4% at a higher mass flow rate. A contour plot of the static pressure and velocity magnitude for a statorless (VTM1) configuration is shown in Fig. 10 (a) and 10 (b), at the maximum efficiency point, corresponding to a mass flow rate 0.7 g/s mass flow rate. The volute case exhibits a well-distributed static pressure, which is not seen in the diffuser case as suggested by Tiwari [10]. Throughout the volute diffuser section, there is the continuous addition of mass flow that results in a uniform distribution of velocity magnitude. In this case, no recirculation has been observed.

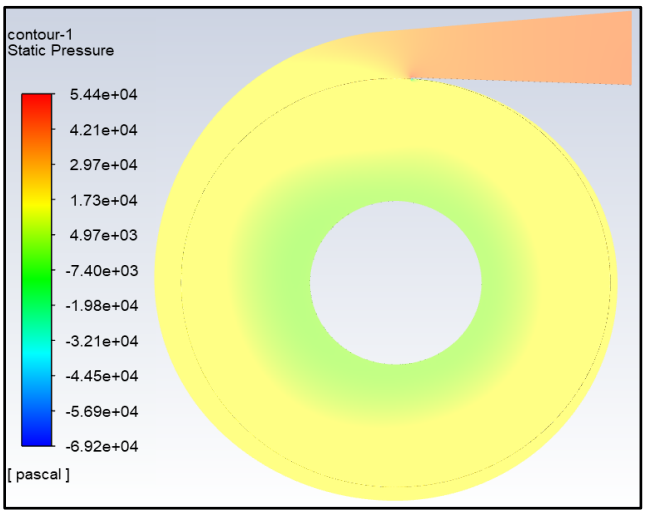

FIGURE 10 (a): STATIC PRESSURE CONTOURS AT 0.7 g/s MASS FLOW RATE

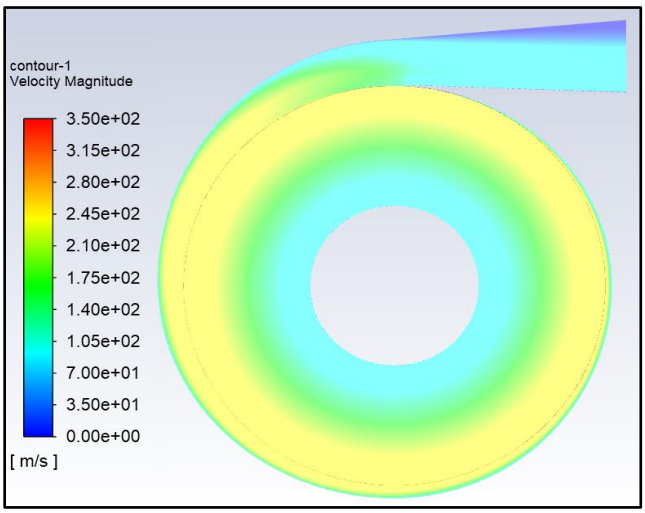

FIGURE 10 (b): VELOCITY MAGNITUDE CONTOURS AT 0.7 g/s MASS FLOW RATE

With regard to the diffuser case, sensitivity is performed for the same rotor model M1 (DR 2.5) at varying the number of diffuser vanes. Four, eight, and twelve vanes diffuser configurations are simulated using rotor model M1 in order to assess their impact on Tesla compressor performance. As explained in section 3.1.2 diffuser, the stator angle is fixed at 3.5°, and each diffuser vane is placed every 1/8th part (8V-45°), so a total of eight diffuser vanes. In the same way, four and twelve-diffuser vane designs are studied without adjusting the rotor (RT-M1) geometry and the stator angle. The diffuser vane numbers are only varied by four-1/4th parts (4V-90°) and twelve-1/12th parts (12V- 30°) as shown in Fig.11.

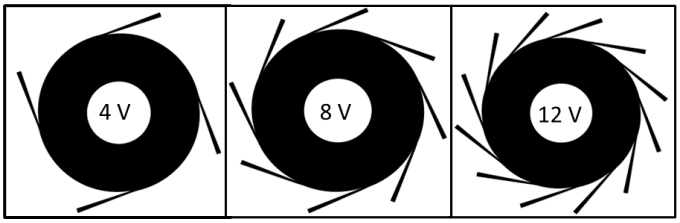

FIGURE 11: STATOR (DIFFUSER VANE) CONFIGURATIONS WITH ROTOR MODEL M1

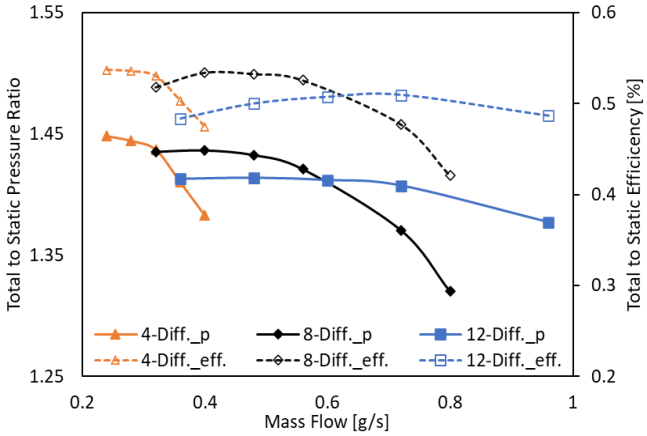

FIGURE 12: TOTAL TO STATIC PRESSURE RATIO AND TOTAL TO STATIC EFFICIENCY VS MASS FLOW RATE AT DIFFERENT NUMBERS OF DIFFUSER VANES (M1 GEOMETRY)

The boundary condition is applied as discussed in previous section 3.1.2 for the other stator configuration number 4 and 12. indicated in Figure 12 the solid shows the pressure ratio while the dashed line shows efficiency. The highest pressure ratio of 1.45 and the highest efficiency of 53.8% is achieved with the 4 diffuser model. By doubling the number of diffuser vanes from four to eight, pressure and efficiency show minor changes, while mass flow rate is almost doubled for the same pressure ratio. However, with a further increase of the diffuser vanes to 12, both pressure ratio and efficiency drop. The peak pressure ratio is now just slightly over 1.4 while efficiency is reduced by 4% points as compared to the 4 diffuser configuration. Hence, this indicates that increasing the diffuser vane area leads to an increase in skin frictional losses, which has an impact on overall performance. Similarly, Chehhat[44] pointed out that in a conventional centrifugal compressor, both pressure ratio and efficiency are affected by increasing the diffuser vanes, and high performance is achieved at a low number of vanes. Nevertheless, such an impact is not universal but is dependent on the specific geometry adopted.

5. CONCLUSION

In this article, bladeless or Tesla compressors are numerically analyzed at different rotor diameters with stator and statorless (volute) configurations. The rotor has been studied independently, which indicates that a larger diameter ratio tends to lead to higher rotor total-to-total efficiency at low mass flow rates. However, maximum rotor efficiency >95% is achieved at rotor diameter ratio ≥ 2.5, where the gap is defined as per optimal Ekman and Reynolds numbers. Pressure is increased proportionally to rotational speed and external radius, which leads to greater pressure ratios with a larger diameter ratio. At the peak point of rotor efficiency, the outlet flow angle is close to tangential. Maintaining this flow angle with a stator configuration is quite challenging, and with a higher angle performance is adversely affected.

The rotor model M1 (DR-2.5) is simulated with diffuser configurations, resulting in a maximum total to static efficiency of 53.5% when the total to static pressure ratio is 1.44. However, for further performance improvement, the statorless (VTM1) configuration is simulated as well using the same rotor model M1. A volute configuration can improve overall performance over 55% of total to static efficiency, as well as produce a total to static pressure ratio of 1.48, which is higher than any vaned diffuser configuration, also allowing for almost double mass flow rates for the same pressure ratio.

The sensitivity on the number of diffuser vanes predicts that a lower number of diffuser vanes would result in a higher pressure ratio and efficiency, but lower mass flow rates. In fact, increasing the number of diffuser passages will lead to frictional losses that degrade overall performance.

According to the numerical results, the volute configuration is the best choice for bladeless compressors from all perspectives, including pressure ratio, efficiency, and mass flow (when high mass flow designs are desirable).

This numerical analysis represents the foundation for the development of a reversible experimental prototype in the near future.

ACKNOWLEDGEMENTS

This project has received funding from the European Union's Horizon 2020 research and innovation programme under the Marie Sklodowska-Curie Grant Agreement No. 861079 ("NextMGT - Next Generation of Micro-Gas Turbines for High Efficiency, Low Emissions, and Fuel Flexibility"). This paper reflects only the authors' view and the Research Executive Agency and the European Commission are not responsible for any use that may be made of the information it contains.

REFERENCES

[1] Tiwari, R., N., Reggio, F., Renuke, A., Pascenti, M., Traverso, A., Ferrari, M.L., 2022, "Performance Investigation of a Bladeless Air Compressor" *J. Eng. Gas Turbines Power*, Vol-144(9) Doi.org/10.1115/1.4054945.

[2] Renuke, A., Vannoni, A., Pascenti, M., and Traverso, A., 2019, "Experimental and Numerical Investigation of Small-Scale Tesla Turbines," *ASME J. Eng. Gas Turbines Power*, 141(12), p. 121011.

[3] Renuke, A., Reggio, F., Traverso, A., and Pascenti, M., 2022, "Experimental Characterization of Losses in Bladeless Turbine Prototype," *ASME J. Eng. Gas Turbines Power*, 144(4), p. 041009.

[4] Zhao, D., Ji, C., Teo, C., & Li, S., 2014, "Performance of small-scale bladeless electromagnetic energy harvesters driven by water or air", *Energy*, 74, 99-108.

[5] L. Magistri, P. Costamagna, A. F. Massardo, C. Rodgers, C. F. McDonald 2002, "A Hybrid System Based on a Personal Turbine (5 kW) and a Solid Oxide Fuel Cell Stack: A Flexible and High Efficiency Energy Concept for the Distributed Power Market", *J. Eng. Gas Turbines Power*, Vol. 124, pp.850-857.

[6] Tesla, N., 1913, "Turbine", US Patent 1061206.

[7] Tesla, N., 1913, "Fluid propulsion" US Patent 1061142.

[8] Tiwari, R., N., Niccolini Marmont, C., A., Reggio, F., Silvestri, P., Traverso, A., and Ferrari, M., L., 2022 "Acoustic Signature Analysis of a Bladeless Blower". Available at SSRN: https://ssrn.com/abstract=4280189.

[9] Rice, W., 1963, "An Analytical and Experimental Investigation of Multiple Disk Pumps and Compressors", *J. Eng. for Power,* 1963. Pp. 191-198.

[10] Tiwari, R., Eleftheriou, K., Ferrari, M.L., Efstathiadis, T., Traverso, A., and Kalfas, A., 2022, "Numerical Investigation of Bladeless Compressor on Different Disk Spaces and Diffuser Configurations" *J. Eng. Gas Turbines Power*, Vol-145(01). Doi.org/10.1115/1.4055705.

[11] Miller, G. E., Etter, B. D., and Dorsi, J. M., 1990, "A Multiple Disk Centrifugal Pump as a Blood Flow Device" *IEEE Transactions on Biomedical Engineering*, vol. 37. No. 2.

[12] Miller, G. E., and Fink, R., 1999, "Analysis of Optimal Design Configurations for a Multiple Disk Centrifugal Blood Pump," *Int. Soc. Artif. Organs Artif. Organs, 23(6), pp. 559–565.*

[13] Rice, W., 2003, "Tesla Turbomachinery," Handbook of Turbomachinery, Logan, E., and Ray, R., Marcel Dekker, New York, Chap. 14.

[14] Epstein, A. H., 2004, "Millimeter-Scale, Micro-Electro-Mechanical Systems Gas Turbine Engines," *ASME J. Eng. Gas Turbines Power*, 126(2), pp. 205–226.

[15] Renuke, A, F. Reggio, P. Silvestri, A. Traverso, M. Pascenti, 2020 "Experimental Investigation on a 3 kW Air Tesla Expander With High-Speed Generator", *ASME Turbo Expo 2020*, virtual, ASME Paper GT2020-14572.

[16] Renuke, A., and Traverso, A., 2022 "Performance Assessment of Tesla Expander Using Three-Dimensional Numerical Simulation" *J. Eng. Gas Turbines Power*, Vol-144(11). DOI.org/10.1115/GT2022-82690.

[17] Crawford, M. E., and Rice, W., 1974, "Calculated Design Data for the Multiple-Disk Pump Using Incompressible Fluid," *ASME J. Eng. Power,* 96(3), pp. 274–282.

[18] Wang, B., Okamoto, K., Yamaguchi, K. and Teramoto, S., 2014, "Loss mechanisms in Shear-Force Pump with Multiple Corotating Disks" *ASME J. Fluids Eng*., 136(8).

[19] Palumbo., J., F., 2002, "Bladeless Turbocharger", US Patent US6368078B1.

[20] Hasinger, S. H., and Kehrt, L. G., 1963, "Investigation of a Shear Force Pump," *ASME J. Eng. Power*, 85, pp. 191–198.

[21] Boyd, K. E., and Rice, W., 1968, "Laminar Inward Flow of an Incompressible Fluid Between Rotating Disks With Full Peripheral Admission," *ASME J. Appl. Mech., 35(2), pp. 229–237.*

[22] Oliveira, M., and Pascoa, J. M., 2009, "Analytical and Experimental Modeling of a Viscous Disc Pump for MEMS Applications," III National Conference on Fluid Mechanics, Thermodynamics and Energy, MEFTE - Braganc¸a, Portugal, Sept. 17–18, Vol. 9

[23] Obayashi, S., Jeong, S.-K., Shimoyama, K., Chiba, K., and Morino, H., 2010, "Multi-Objective Design Exploration and Its Applications*," Int. J. Aeronaut. Space Sci.,* 11(4), pp. 247–265.

[24] Stepanoff A., J., 1957, "Centrifugal and axial flow pumps: theory, design and applications", *New York: John Wiley & Sons Inc*, 1957. p. 111–4.

[25] Mohtar, H., 2011 "Effect of Diffuser and Volute on Turbocharger Centrifugal Compressor Stability and Performance: Experimental Study". *In: Oil & Gas Science and Technology 66.5 (2011), pp. 779–790. doi: 10.2516/ogst/2011139.*

[26] Dumitrescu, O., Fetea, G., and Gherman , B., 2017 "Influence of the volute design on performances of a centrifugal compressor," *2017 International Conference on Energy and Environment (CIEM)*, 2017, pp. 432-436, DOI: 10.1109/CIEM.2017.8120870.

[27] De Souza, B., Niven, A., & McEvoy, R., 2010 "A numerical investigation of the constant-velocity volute design approach as applied to the single blade impeller pump", *Journal of Fluids Engineering*, 132(6).

[28] Pan, D., Whitfield, A., & Wilson, M. (1999). Design considerations for the volutes of centrifugal fans and compressors. Proceedings of the Institution of Mechanical Engineers, Part C: Journal of Mechanical Engineering Science, 213(4), 401-410.

[29] Yu, Y., Ren, W., & Liu, J., 2019, "A new volute design method for the turbo air classifier", *Powder Technology*, vol- 348, 65-69. DOI.org/10.1016/j.powtec.2019.03.015

[30] Galindo, J., Hoyas, S., Fajardo, P., Navarro, R., 2013, "Set-Up Analysis and Optimization of CFD Simulations for Radial Turbines", *Engineering Applications of Computational Fluid Mechanics,* 7:4, 441-460, DOI: 10.1080/19942060.2013.11015484.

[31] Zhu, Y., and Jiang, P., 2014, "Experimental and Numerical Investigation of the Effect of Shock Wave Characteristics on the Ejector Performance," *Int. J. Refrig., 40, pp. 31–42*.

[32] Croquer, S., Poncet, S., and Aidoun, Z., 2016, “Turbulence Modeling of a Single-Phase R134a Supersonic Ejector. Part 1: Numerical Benchmark,” Int. J. Refrig., 61, pp. 140–152.
[33] Menter, F. R., 1992, “Influence of Freestream Values on k-Omega Turbulence Model Predictions*”, AIAA J., 30(6), pp. 1657–1659.*
[34] Wilcox D.,C., 1988, “Reassessment of the scale-determining equation for advanced turbulence models”, *AIAA Journal 26(11):1299-1310.*
[35] Menter F., R., “A comparison of some recent eddy-viscosity turbulence models”, J Fluids Eng 1996; 118: 514–519.
[36] Zamiri, A., Lee, B., J., and Chung, T., J., 2017 “Numerical evaluation of transient flow characteristics in a transonic centrifugal compressor with vaned diffuser,” Aerospace Science and Technology, vol. 70, pp. 244–256.
[37] Tomboulides, A., Aithal, S. M., Fischer, P. F., Merzari, E., Obabko, A. V., & Shaver, D. R., 2018. “A novel numerical treatment of the near-wall regions in the k− ω class of RANS models”, *International Journal of Heat and Fluid Flow*, 72, 186-199.
[38] Peric, M., 2004, “Flow simulation using control volumes of arbitrary polyhedral shape”, ERCOFTAC Bulletin, No. 62 (2004).
[39] Cumpsty, N. A., and Horlock, J. H., 2006, "Averaging Nonuniform Flow for a Purpose." ASME. *J. Turbomach*, Vol-128(1): 120–129. https://doi.org/10.1115/1.2098807
[40] Zhao Z, Guo Z, Qian Z, Cheng Q. “Performance improvement of an axial-flow pump with inlet guide vanes in the turbine mode. Proceedings of the Institution of Mechanical Engineers, Part A”: *Journal of Power and Energy. 2020;234(3):323-331. doi:10.1177/0957650919858842*
[41] Zhou L, Xi Y and Cai Y. 2008 “Experimental study on the influence of diffuser and inlet guide vane for the performance of centrifugal compressor”. *Exp Techniques 2008; 32: 26–33.*
[42] Liu Y, Tan L, Liu M, 2017 “Influence of prewhirl angle and axial distance on energy performance and pressure fluctuation for a centrifugal pump with inlet guide vanes”. *Energies 2017; 10: 695.*
[43] Wilkes, J., Pettinato, B., Kurz, R., Hollingsworth,J., Zhang, D., Taher, M., Kulhanek, C., Werdecker, F., Büche, D.,Talabisco, G., 2019 "Centrifugal Compressors" *Compression Machinery for Oil and Gas, Gulf Professional Publishing,Pages 31-133,ISBN 9780128146835. DOI.org/10.1016/B978-0-12-814683-5.00003-1.*
[44] Chehhat, A., Si-Ameur, M., Boumeddane, B., Abo-Serie, E., & Boulahrouz, S., 2016, “Numerical investigation of diffuser solidity effect on turbulent airflow and performance of the turbocharger compressor”, *Applied and Computational Mechanics*, vol. 10, no. 2, p. 79-96.